IEEE Access
Multidisciplinary ⋮ Rapid Review ⋮ Open Access Journal

Received September 19, 2020, accepted October 8, 2020, date of publication October 13, 2020, date of current version October 28, 2020.

Digital Object Identifier 10.1109/ACCESS.2020.3030796

Scanning Strategy of Deviation-Boundary Prediction Based on Probe Dynamics

WEIKANG ZHENG, ZHIGANG LIU, (Member, IEEE), JUNKANG GUO, (Member, IEEE), AND JUN HONG, (Member, IEEE)

Key Laboratory of Education Ministry for Modern Design and Rotor-Bearing System, School of Mechanical Engineering, Xi'an Jiaotong University, Xi'an 710049, China

Corresponding author: Zhigang Liu (mezgliu@mail.xjtu.edu.cn)

This work was supported in part by the Natural Science Foundation of China under Grant 51875447 and Grant 51805419, in part by the Fundamental Research Funds for the Central Universities under Grant xzy022019073, and in part by the China Postdoctoral Science Foundation funded project under Grant 2018M631147.

ABSTRACT Contact scanning probes have higher accuracy than non-contact probes in industrial applications. But changes of the measured surface and adjustment of velocity and acceleration may cause random measurement deviations, which are mainly determined by dynamic characteristics of the probe system. To realize the prediction of measurement deviations related to scanning parameters, this paper proposes a simpler detection method of dynamic performance. In this article, the dynamic response characteristics of the probe to diverse external stimuli are studied theoretically and experimentally on the basis of the original probe design. Under different scanning variables including the amplitude, spacing and shape of the surface, velocity and acceleration, the integration of the second-order vibration model and external excitation forms the theoretical basis for quantitative analysis of the system response, and numerical simulation and three sets of experiments are designed to effectively verify the deviation distribution of the system response caused by different scanning parameters in the time and frequency domains.

INDEX TERMS Scanning probe, velocity and acceleration, external excitation, natural frequency, deviation-boundary prediction.

I. INTRODUCTION

Contact scanning probes have higher measurement accuracy than non-contact probes, and are widely used in industrial measurement. However, higher scanning velocity may bring greater measurement deviations [1], [2] in high-efficiency measurement applications.

Scanning velocity/acceleration is an important source of dynamic error in probe measurement, and the identification of error sources and the evaluation of deviations have long been concerned [3]. The natural frequency of some flexible probes is usually around 100∼600 Hz [4]–[9], making the probe response very sensitive to the scanning velocity and acceleration. Farooqui and Morse [10] proposed a method based on the shape detection of standard samples. By changing the scanning parameters such as velocity and scanning directions to study the dynamic performance of CMM (Coordinate Measuring Machines), it was found that changes in scanning velocity may lead to significant deviations. Pereira and Hocken [11] experimented with the high-velocity measurement performance of the CMM by using the calibrated ring sample, and proposed a first-order approximate scanning model to well compensate the dynamic error. Krajewski and Woźniak [1] designed an angle sample to better demonstrate the influence of different scanning velocity on the measurement accuracy of active or passive probes from the frequency-amplitude domain. Later, the sample is improved with a pressure sensor [2] to identify and estimate the source of dynamic errors by detecting the contact pressure of the stylus. These typical methods mainly rely on various forms of samples to analyze the deviations under different scanning velocity/acceleration scenarios, which are effective for specific probes and specific tested parts.

However, the measurement object of the scanning probe is not unique, but a surface or movement with complex and diverse characteristics, including spacing, amplitude, and curvature, etc.. The above methods cannot solve these challenging tasks well. External auxiliary detection equipment,

The associate editor coordinating the review of this manuscript and approving it for publication was Usama Mir.

such as laser interferometer [12], piezoelectric ceramic converter [13] are also often used in these scenarios, but they are expensive and complicated to implement. Pollastri's contribution [14] seems more effective. In the gear error detection, he proposed the concept of the selection domain for the waviness-scanning velocity of the sample, which is used to achieve a reasonable balance between the scanning velocity and measurement uncertainty. This selection strategy is relatively enlightening. Although the dynamic characteristics of the probe system are decisive in the selection of scanning parameters, the existing methods are more to study the probe's response without effectively combining the internal dynamic characteristics of the probe with external excitations, which can promote the establishment of a mathematical relationship between the scanning parameters including velocity/acceleration, the surface or motion characteristics of the sample, and the natural frequency and damping ratio of the probe. Thus, the unified analysis of the internal and external parameters of the probe during scanning will enable the prediction and evaluation of the system response and deviations for most scanning parameters. In this case, various forms of standard samples are not necessary.

Based on the design of a flexible probe [11], [15], this paper studies the system response characteristics generated by the coupling of the dynamic characteristics of the probe system and diverse external excitations, including different surface or motion, velocity and acceleration. The constructed mathematical mapping between the external excitation variables and the system deviation provides a predictive scanning strategy for the dynamic scanning of the probe, so as to avoid the measurement deviation caused by improper selection of scanning velocity and acceleration.

II. DYNAMIC PERFORMANCE OF THE PROBE SYSTEM

The flexible probe used by the scanning strategy research is shown in Fig. 1 It uses a monolithic compliant mechanism as the force-deformation structure, and uses capacitive displacement sensors to monitor the z-direction deformation of the three cantilevers **B**, **D**, and **F** in real time. During the scanning, the stylus of the probe generates continuous vibration along the direction of the contact force, and produces real-time responses on the three cantilevers. Because of the dynamic characteristics of the probe system, there is not only a basic linear relationship between the continuous vibration of the probe ball and the displacement response of the cantilever in the scanning measurement, but also the dynamic response deviations determined by the natural frequency and damping ratio of the system. The deviations are inspired by the scanning velocity/acceleration and the characteristics of the measured surface or motion. A simplified diagram of the dynamics of the probe system is shown in Fig. 1(b).

A. 2ND ORDER VIBRATION MODEL OF PROBE

The second-order vibration model is a typical mass-spring-damped vibration system. The system input is the contact force $\boldsymbol{F}$, which results in the ball displacement s or the offset

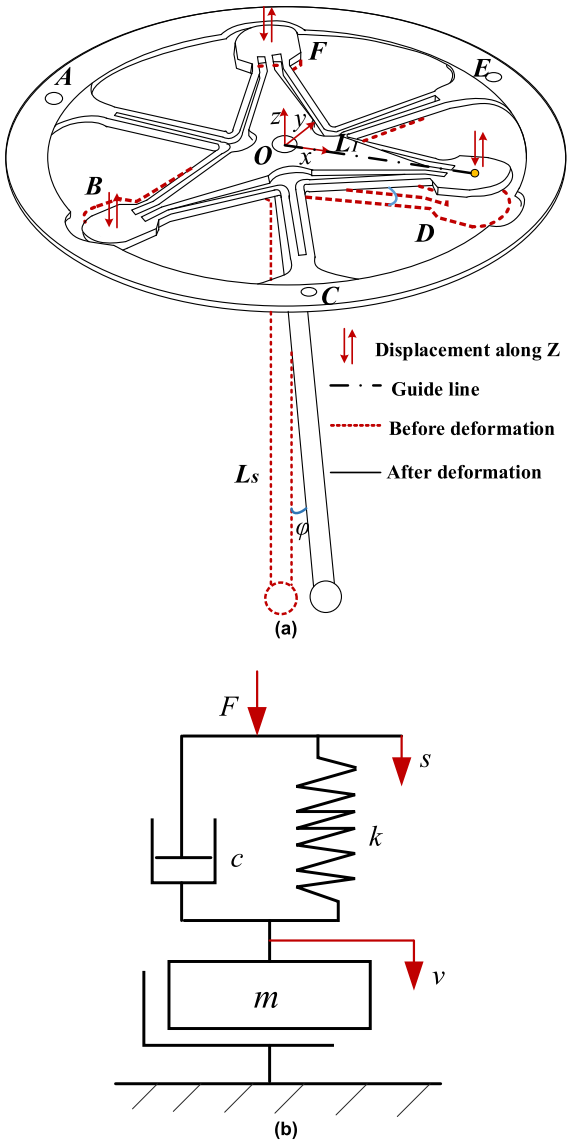

FIGURE 1. Vibration analysis of the probe system. (a) Deformation in the scanning. (b) Model simplification.

angle φ. The system output is the cantilever vertical displacement v or the center-based offset angle γ. And there is a clear conversion relationship between the corresponding angle and displacement. As shown in Fig. 1(a), L_s is the effective length of the stylus, L_1 is the distance from the monitoring point of the cantilever displacement to the geometric center $\boldsymbol{O}$, and J_{eq} is the equivalent moment of inertia. In addition, $\gamma = v/L_1$, $k_{sp} = k_d v/\gamma$, where k_{sp}, k_d are rotational and linear stiffness of the cantilever, respectively. The second-order vibration model of the system can be derived based on the deformation principle of the three-dimensional structure of the probe, as follows.

$$J_{eq}\ddot{\gamma} + c\dot{\gamma} + k_{sp}\gamma = FL_s \tag{1}$$

where c is the viscous damping coefficient. Equation (1) can be then transformed into Equation (2), and the transfer

function G_s of the probe system is therefore derived as Equation (3).

$$\ddot{v} + c/J_{eq}\dot{v} + k_{sp}/J_{eq}v = FL_sL_1/J_{eq} \tag{2}$$

$$G_s = \frac{L_sL_1}{J_{eq}s^2 + cs + k_{sp}} \tag{3}$$

B. ANALYSIS OF EXTERNAL EXCITATION AND SYSTEM RESPONSE OF THE PROBE

The probe in this article is used on the machine tool to detect the spatial pose of the machine motion. The independent design and manufacturing of the probe provides convenience for the dynamic research. For any mechanical system, the natural frequency and damping ratio determine the characteristics of the system response to any external excitation, and ultimately cause the large or small measurement deviations under different scanning parameters. Therefore, the dynamic model of the probe can be used to effectively construct the mathematical mapping between the scanning parameters and the response deviations, and the boundary of the measurement deviations can be predicted under the actual working conditions, finally contributing to a better scanning strategy.

1) CHARACTERISTIC DESCRIPTION OF THE MEASURED SURFACE OR MOTION

There are about 40 characteristic parameters of dynamic motion or surface topography [16], [17], which can be divided into three categories of height, interval space and shape, which reflect the ups and downs of the topography, the distance between the peaks or valleys, and the curvature characteristics of the shape, respectively, as shown in Fig. 2(a).

The sine function is used to describe the ideal measured surface or motion, as in Equation (4), where A represents the amplitude of the topography, x represents the distance swept by the probe along the scanning direction, and l represents the periodic distance.

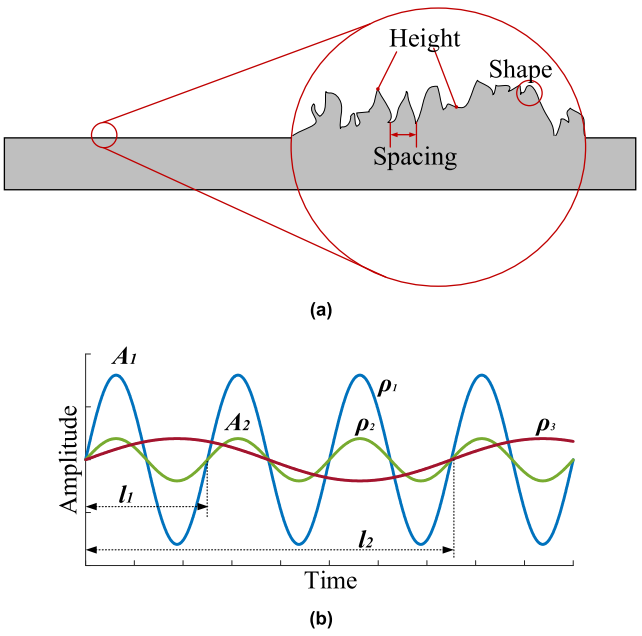

FIGURE 2. Characterization of the measured surface or movement. (a) Characteristic analysis. (b) Mathematical description.

$$f = A\sin(\frac{2\pi}{l}x) \tag{4}$$

The sinusoidal curves under different surfaces can be simulated by adjusting the amplitude A and the spacing l, and the two also determine the curvature characteristic ρ of the curve. When the change of the measured surface or motion is very small and approximate to an ideal plane, both the amplitude A and the spacing l will be infinitely large; when the change is very sharp, the amplitude A will increase and the spacing l will decrease, respectively. It should be noted that the characteristics of the actual measured object are complex and diverse, so the most sensitive surface features can be used as the basis for deviation evaluation.

2) RESPONSE ANALYSIS UNDER SCANNING VELOCITY

The excitation signal of the probe system is expressed by the continuous contact force $\boldsymbol{F}(t)$ formed by the measured surface or motion, as described in Equation (5), where k_s is the touch stiffness of the probe in the scanning. Then the frequency response of the probe system $X_o(s)$ can be obtained from the product of the transfer function (Equation (3)) and the Laplace transform of the excitation signal $L[F(t)]$. Further, the time response of the system $x_o(t)$ is derived from the inverse Laplace transform of Equation (6).

$$F(t) = A\sin\frac{2\pi v_0 t}{l}\cdot k_s \tag{5}$$

$$\begin{aligned} X_o(s) &= G(s)\cdot\frac{2\pi Av_0lk_s}{l^2s^2 + 4v_0^2\pi^2} \\ &= \frac{2\pi Av_0lk_sL_sL_1}{(J_{eq}s^2 + cs + k_{sp})(l^2s^2 + 4v_0^2\pi^2)} \end{aligned} \tag{6}$$

where $c = 2\xi w_nJ_{eq}$, $w_n = \sqrt{k_{sp}/J_{eq}}$, $w_d = w_n\sqrt{1-\xi^2}$, and ξ is damping ratio, w_n, w_d are the natural frequency and resonance frequency of the system, respectively.

$$x_0(t) = \frac{2\pi Ack_sl^3L_sL_1ve^{-ct/2/J_{eq}}Q_1 - Q_2}{Q_3} \tag{7}$$

where

$$\begin{aligned} Q_1 &= \cosh(\frac{t}{J_{eq}}\sqrt{\frac{c^2}{4} - J_{eq}k_{sp}}) \\ &\quad - \frac{J_{eq}\sinh(\frac{t}{J_{eq}}\sqrt{\frac{c^2}{4} - J_{eq}k_{sp}})(\frac{c-2}{2J_{eq}} - \frac{4\pi^2v_0^2J_{eq}^2 - k_{sp}J_{eq}l^2}{cJ_{eq}l^2})}{\sqrt{\frac{c^2}{4} - J_{eq}k_{sp}}} \\ Q_2 &= 4A\pi^2J_{eq}k_sL_sL_1l^2v_0^2\sin(\frac{2\pi v_0t}{l}) \\ &\quad - Ak_sk_{sp}L_sL_1l^4\sin(\frac{2\pi v_0t}{l}) \\ &\quad + 2A\pi ck_sL_sL_1l^3v_0\cos(\frac{2\pi v_0t}{l}) \\ Q_3 &= 16\pi^4J_{eq}^2v_0^4 + 4\pi^2c^2l^2v_0^2 - 8\pi^2J_{eq}k_{sp}l^2v_0^2 + k_{sp}^2l^4 \end{aligned}$$

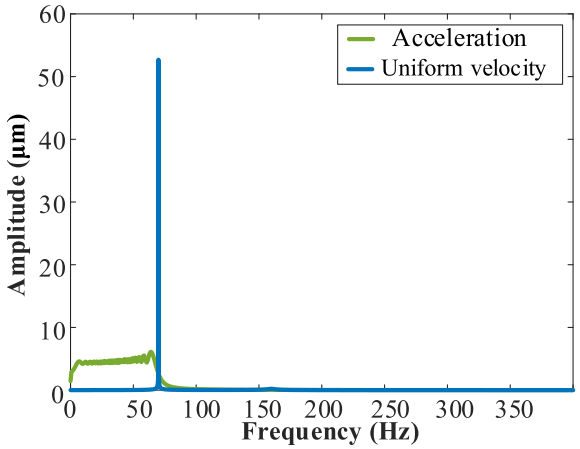

FIGURE 3. Comparison of spectral characteristics between acceleration and uniform velocity.

TABLE 1. Parameters in time domain response function.

Parameters	Value
J_{eq}	0.000022 N·m^2
k_s	574 N/m
k_{sp}	22.234 N/rad
ξ	0.02
L_s	50 mm
L_1	26 mm
c	1.41e-4 N·m^2·Hz
w_n	160 Hz

$\boldsymbol{Q_1/Q_3}$, $\boldsymbol{Q_2/Q_3}$ represent the transient response of the system and the steady-state response, respectively. There is a strong coupling relationship between sinusoidal waviness and velocity, especially in the steady-state response, where the velocity has made obvious non-linear modulation to the sinusoidal waviness. The higher the velocity, the greater the deviation between the amplitude of the steady-state response and the true value. From the spectrum analysis, the dominant frequency and the corresponding amplitude in the response signal spectrum show an increasing trend when the scanning velocity increases from small to large.

3) RESPONSE ANALYSIS UNDER SCANNING ACCELERATION

Taking sine waviness as the measurement object, the system response under scanning acceleration is a sine wave with continuously changing frequency. As shown in Fig. 3, the two processes of the scanning acceleration and uniform scanning after the acceleration present two completely different spectral characteristics. In the acceleration stage, there is a wide frequency band without clear main frequency; while in the uniform velocity stage, the main frequency is significant and there is no additional frequency. The acceleration process in scanning measurement cannot be avoided, and the deviation in response amplitude caused by the acceleration difference needs to be clarified.

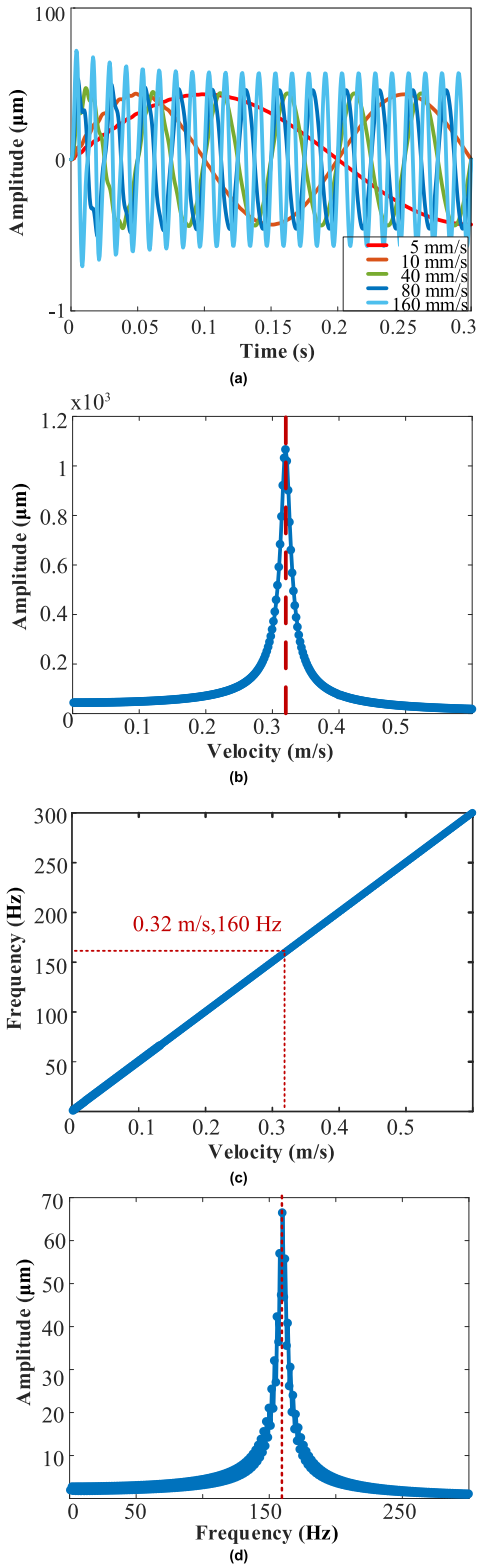

FIGURE 4. System response under different scanning velocity. (a) Amplitude oscillation. (b) Changes of steady-state amplitude change. (c) Main frequency under variable velocity and (d) corresponding amplitudes.

The contact force during accelerated scanning is expressed by $\boldsymbol{F}(t)$, and the distance x in Equation (4) is expressed by $at^2/2$, thus Equation (8) is derived. The composite function

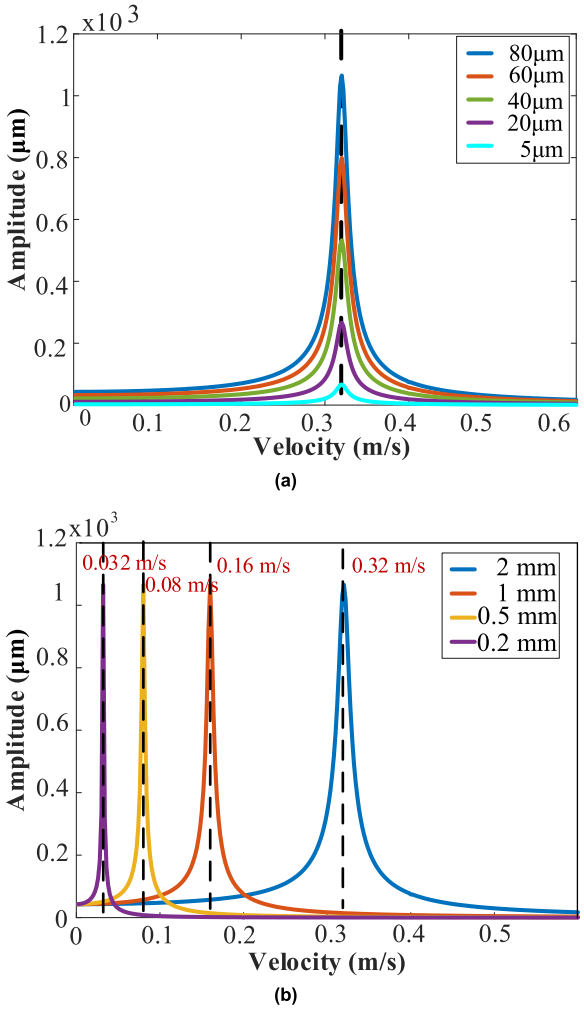

FIGURE 5. The velocity-amplitude curve under (a) the amplitude *A* and (b) the spacing *l*.

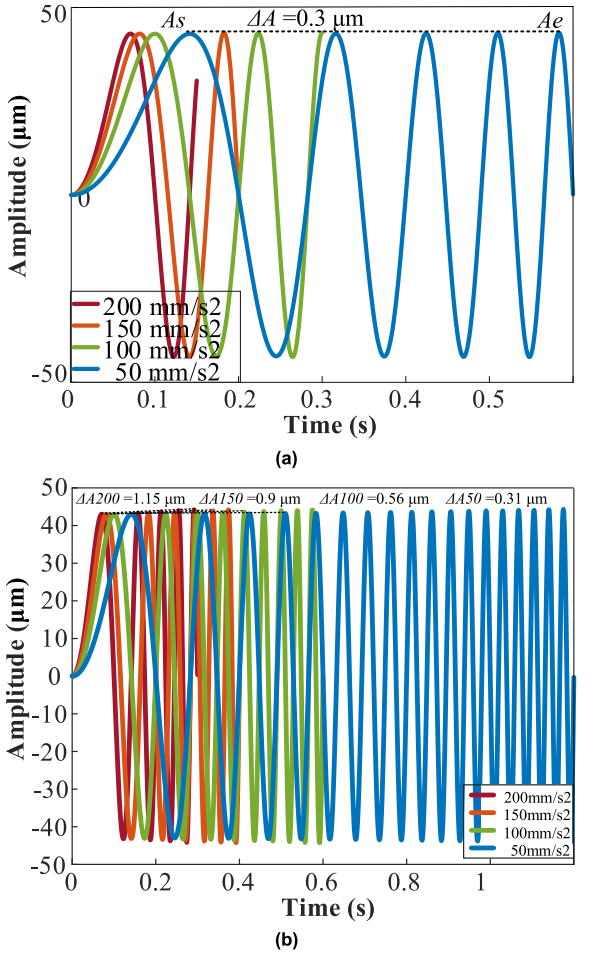

FIGURE 6. Accelerating excitation and response deviation (a) 30 mm/s and (b) 60 mm/s.

cannot obtain an accurate frequency expression through the Laplace transform, so the time response of the system $x_o(t)$ is processed as the time convolution of the excitation signal $\boldsymbol{F}(t)$ and the transfer function $L^{-1}[G]$, as in Equation (9).

$$F(t) = A \sin \frac{a\pi t^2}{l} \cdot k_s \tag{8}$$

$$x_0(t) = F \otimes L^{-1}[G(s)] \tag{9}$$

where a is the acceleration, and t is the acceleration time.

III. SIMULATION ANALYSIS OF PROBE SYSTEM RESPONSE

The possible influence of the scanning parameters on the system dynamic response is mainly determined by the first-order natural frequency of the probe. It can be said that the first-order natural frequency restricts the improvement of the scanning efficiency of the probe. With the help of the constructed system response function (Equation(6) and (8)), the numerical simulation shows the clear deviation distribution of the probe scanning.

A. DEVIATION DISTRIBUTION UNDER UNIFORM SCANNING

A sine surface with an amplitude of 80 μm and a single period of 2 mm is used as the measurement object, and a velocity of 2-600 mm/s is set to obtain the system response. Table 1 shows the parameter assignments in the response function, among which the first-order natural frequency is obtained by FEA (Finite element analysis). Fig. 4(a) shows the velocity-amplitude curves in the velocity range of 5-160 mm/s. The amplitude curve at the beginning is coupled with the transient response fluctuation, and the amplitude increases as the velocity becomes larger. And the amplitude in the steady-state period has also increased. Therefore, the amplitude of the steady-state response curve of the system in the velocity range of 2-600 mm/s is calculated as shown in Fig. 4(b). The steady-state amplitude distribution of the probe system can be divided into three stages: in the first stage **I**, the amplitude basically remains stable, showing a slow and tiny increase; in the second stage **II**, the amplitude increases sharply, and reaches the peak at about 320 mm/s, the system resonates (160 Hz); in the third

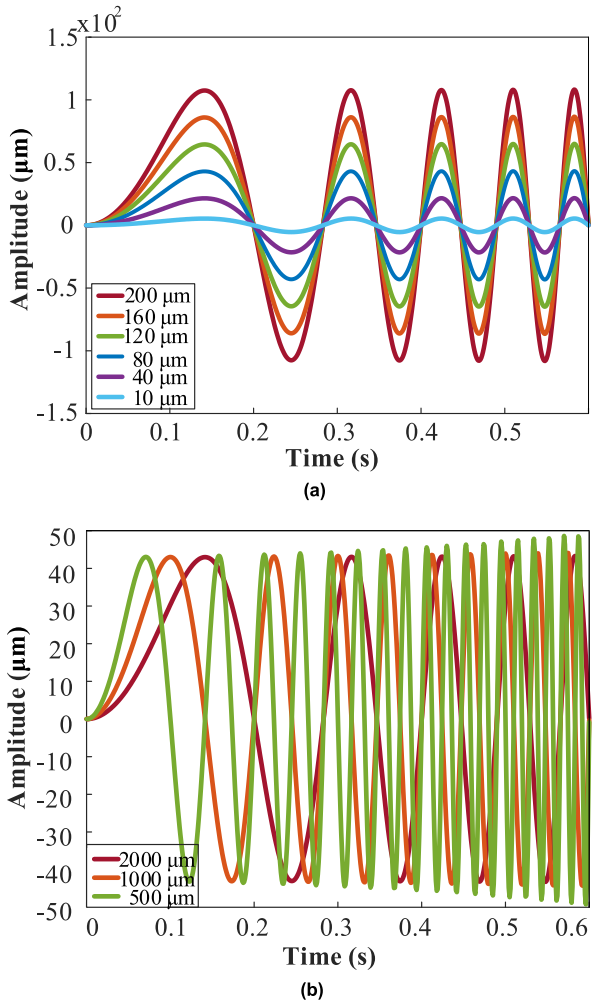

FIGURE 7. The acceleration-amplitude cure under (a) the amplitude A and (b) the spacing *l*.

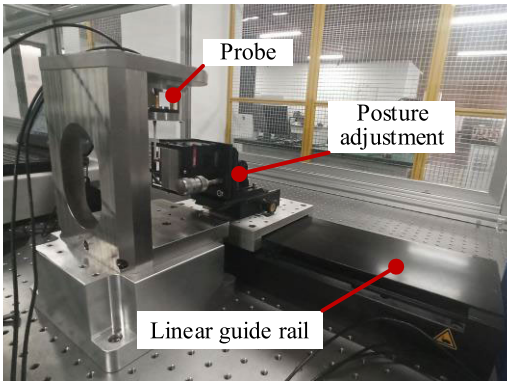

FIGURE 8. Experimental platform for scanning verification.

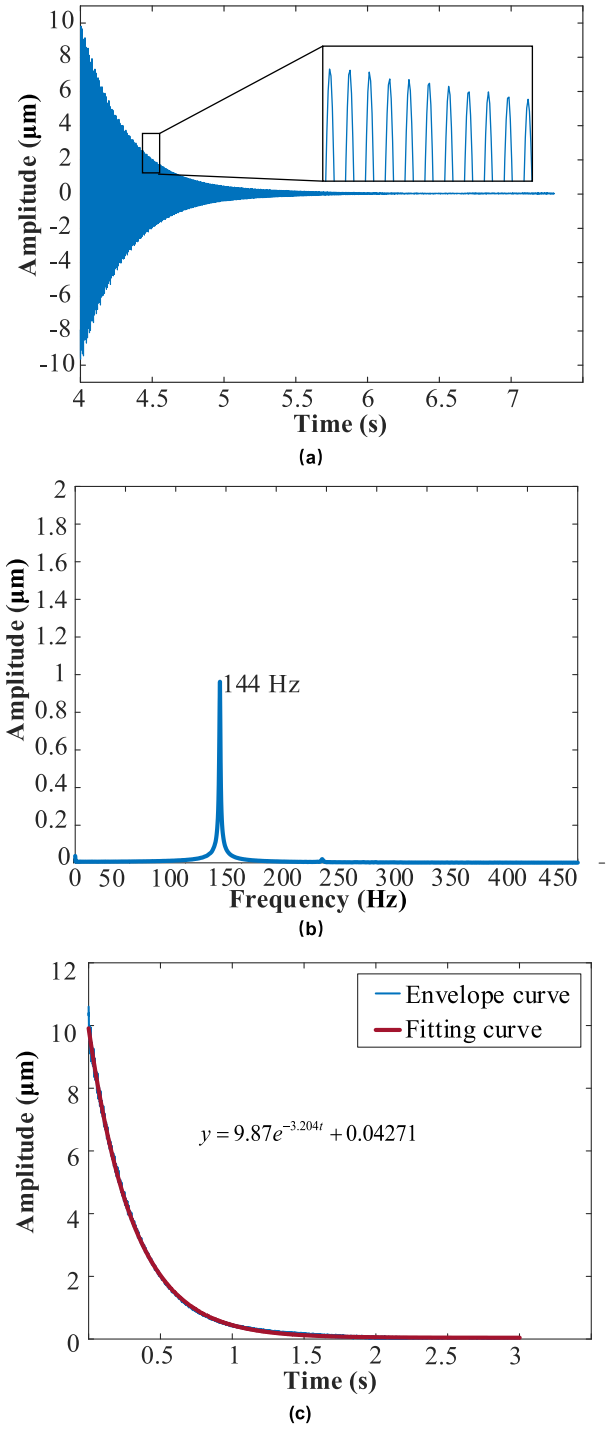

FIGURE 9. Dynamic system identification of the probe prototype (a) free attenuation curve. (b) Frequency spectrum. (c) Envelope and fitting curve of attenuation.

stage **III**, the steady-state amplitude after the peak decays nonlinearly to zero. When the amplitude of the velocity-amplitude curve begins to increase non-linearly, the measurement result has begun to distort, which means that the resonance effect begins to appear. The internal mechanism of the change of the velocity-amplitude curve is revealed by the velocity-main frequency curve in Fig. 4(c) and the main frequency-amplitude curve in Fig. 4(d). The main frequency of the response at different velocity changes linearly, and the amplitude corresponding to the main frequency is similar to the velocity-amplitude curve, showing a significant

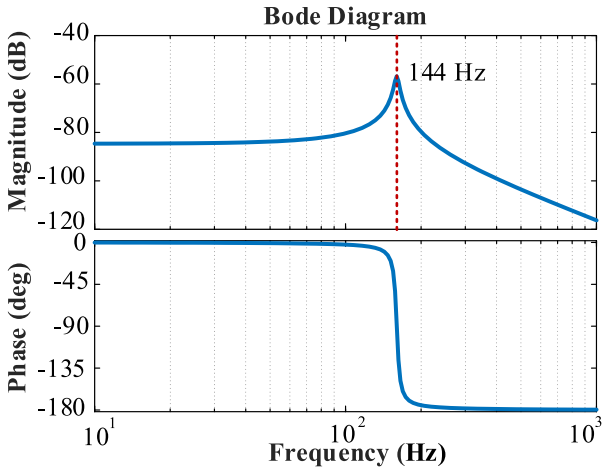

FIGURE 10. Bode diagram of the probe.

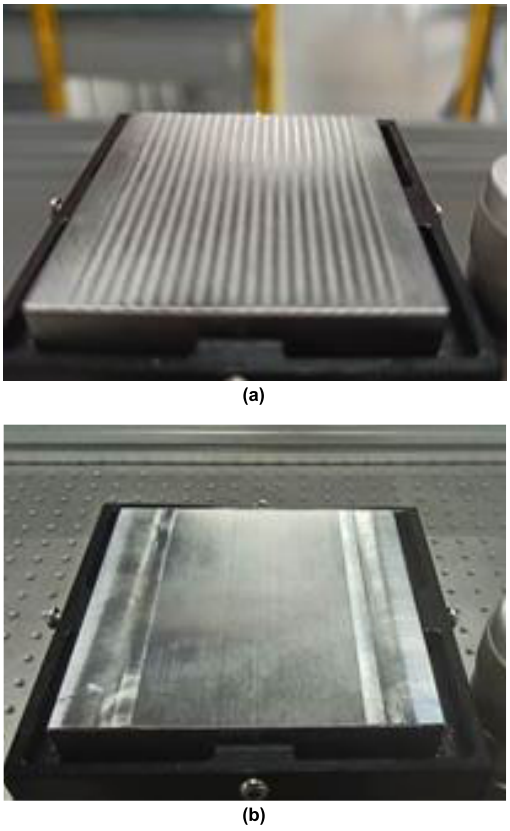

FIGURE 11. Machined surface. (a) Amplitude A = 80-100 μm, spacing l = 2 mm. (b) Amplitude A = 200 μm, spacing l =30 mm.

non-linear change. The spectral amplitude also reaches the maximum at a velocity of 320 mm/s, which corresponds to the first-order natural frequency of the probe 160 Hz. Therefore, if the steady-state deviation during scanning of the probe is set to 1.0 μm, the velocity interval can be selected as (0, 48] mm/s according to the velocity-amplitude curve.

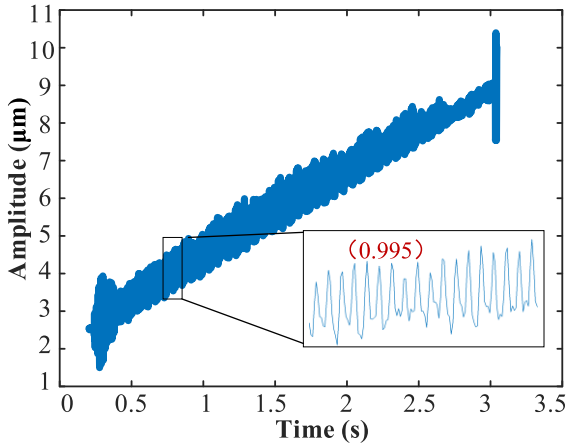

FIGURE 12. Axial runout of linear guide.

The natural frequency of the probe system determines or limits the upper limit of the scanning velocity. The amplitude deviation caused by the scanning velocity is not concentrated near the fixed frequency, but attenuates nonlinearly to both sides with the fixed frequency as the center. Different measurement tasks have different preferences for errors, and the maximum allowable scanning velocity under different requirements can be selected specifically, so as to take into account scanning efficiency and accuracy. This analytical method connects the scanning parameters, measurement deviations and system dynamic performance, thus realizing the estimation of measurement deviations and the optimization of scanning strategies.

The amplitude A and spacing l of the measured surface or motion also affect the measurement deviation. The larger the amplitude A is, the more obvious the oscillation deviation of the system response curve at the same velocity will be; the smaller the distance l is, the narrower the stage **I** will be. Fig. 5(a) shows the velocity-amplitude curve of the system when the topography amplitude changes from 80 to 5 μm. When the amplitude is 80, 60, 40, 20, 5 μm, the resonance peaks are all at the velocity of 0.32 m/s. As the amplitude changes from 80 to 5 μm, the resonant peak of the system decreases sharply along with the smoother stage **I**. The upper limit of the scanning velocity under the allowable measurement deviation can be higher at low amplitudes.

Fig. 5(b) reflects the response of the probe to sinusoidal signals at different intervals. The peaks of the velocity-amplitude curves when the spacing is 2 mm, 1 mm, 0.5 mm, and 0.2 mm are 0.32 m/s, 0.16 m/s, 0.08 m/s and 0.032 m/s, respectively. The smaller the distance l, the smaller the velocity to achieve the resonance effect, that is, the main peak of amplitude, which shows the left shift of the main peak, and leads to an increase in the measurement deviation of the first stage of the velocity-amplitude curve. For measuring objects with drastic changes in surface or motion, the proposed method can better match the scanning velocity to meet the needs of measurement accuracy.

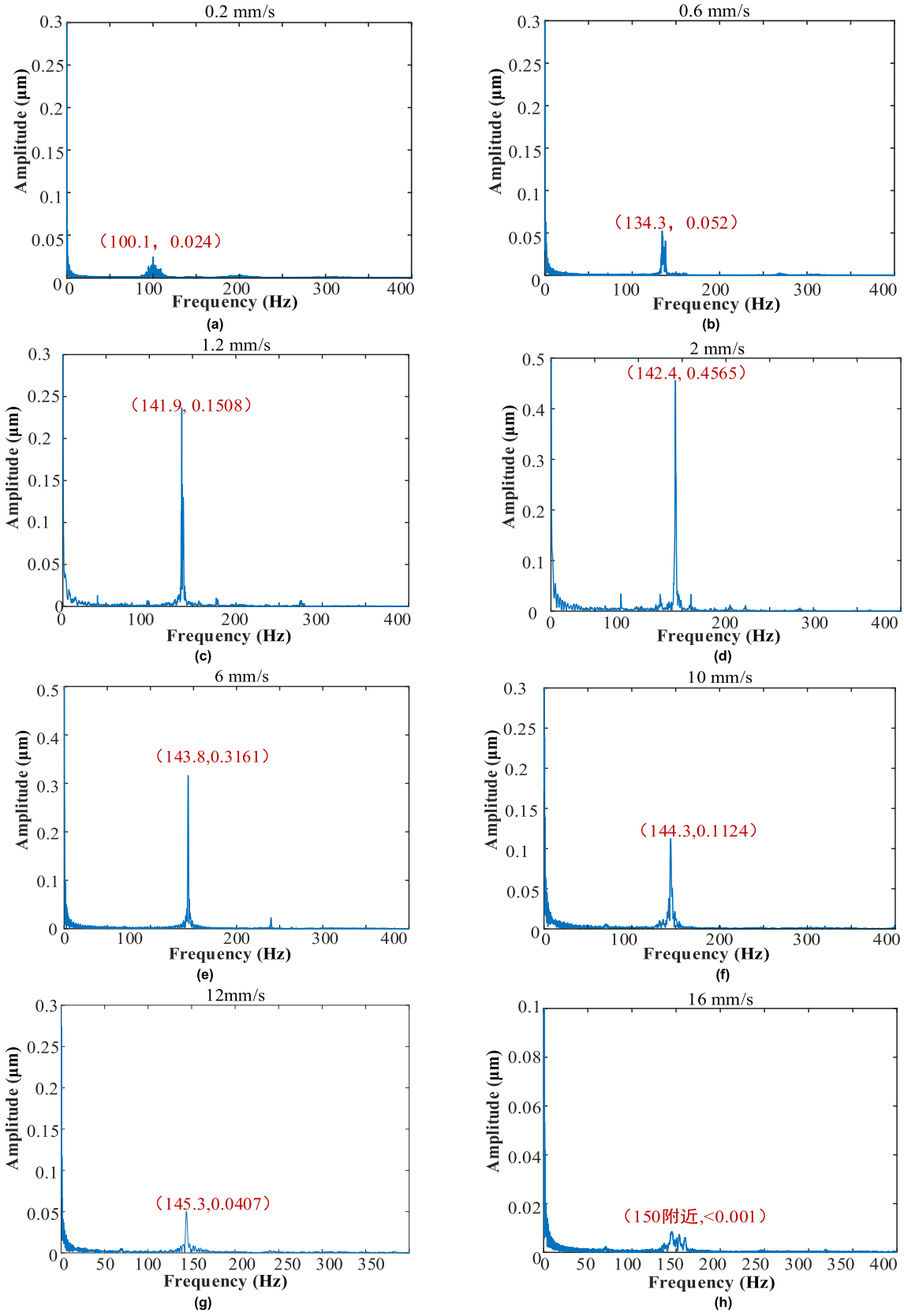

FIGURE 13. Spectral characteristics at different velocity.

B. DEVIATION DISTRIBUTION UNDER ACCELERATED SCANNING

The acceleration range adopted in this part is between 50 - 200 mm/s^2. Fig. 6(a) reflects the system response curve under acceleration excitation before the scanning velocity reaches 30 mm/s. The measured sinusoidal surface is set to an amplitude of 80 μm and periodic length of 2 mm.

The probe sweeps 5 sine peaks. The deviation between the 5th peak A_e and the 1$_{st}$ peak A_s is 0.3 μm with the acceleration set to 50 mm/s^2, and the deviation in the uniform scanning for comparison is close to zero. When scanning with a large acceleration, the scanning velocity is too small to include 5 sine peaks, so the peak fluctuation cannot be observed. But when the velocity is larger, the deviation in the same situation is bigger. Fig. 6(b) further shows the acceleration response curve at a velocity of 60 mm/s. From the amplitude envelope represented by the black dashed line, the amplitude shows an approximately linear increase under different accelerations. In terms of the amplitude deviation between the 5th and the 1st peak, ΔA at accelerations of 200 mm/s^2, 150 mm/s^2, 100 mm/s^2, and 50 mm/s^2 are 1.15 μm, 0.9 μm, 0.56 μm, 0.31μm, respectively. However, from the analysis of the whole acceleration process, the generated ΔA are 1.15 μm, 1.16 μm, 1.22 μm, and 1.32 μm, respectively. It can be seen that the amplitude deviations at this time has undergone opposite changes, and the peak deviation at small acceleration is larger, for the probe has swept a longer distance x.

The spacing feature is closely related to the frequency in the excitation response. At the same velocity, the larger the distance l is, the smaller the dominant frequency (or frequency band) of the response signal will be, thus closer to the resonance frequency. In Fig. 7, compared to the case where the distance l is at 2000 μm and 1000 μm, the response amplitude at $l = 500$ μm shows obvious increase. In this case, only when the scanning velocity is within the selected interval, can such a significant increase in amplitude deviation be avoided.

In short, if the same distance is scanned with different accelerations, the amplitude deviation will increase as the acceleration increases. However, if the scanning is performed at a constant velocity after reaching the specified velocity, the amplitude deviation in the distance swept by the acceleration will decrease as the acceleration increases. For those high-amplitude and small-pitch surfaces or waves, it is necessary to consider the acceleration, velocity, acceleration distance, and uniform scanning distance based on the calculated error boundary.

IV. VIBRATION MODEL IDENTIFICATION AND EXPERIMENTAL VERIFICATION

A. SECOND-ORDER VIBRATION MODEL IDENTIFICATION

The high flexibility and limited linear elastic range of the probe make it difficult to apply conventional vibration identification methods such as hammering. This paper proposes a method of free decay curve. In the experiment shown in Fig. 8, the posture platform is used to make the probe ball and the mirror surface have a soft contact, which produces a displacement of 20-40 μm in the normal direction. Then the linear guide moves at a uniform velocity in one direction to achieve the final separation of the two, thereby obtaining the attenuation curve of free vibration in Fig. 9(a). After the free decay curve is Fourier transformed, the first-order natural frequency in Fig. 9 (b) is obtained, which is 144 Hz. Further, $\xi w_n = 3.204$ is obtained after fitting the envelope of the attenuation curve, and the damping ratio is 0.0225.

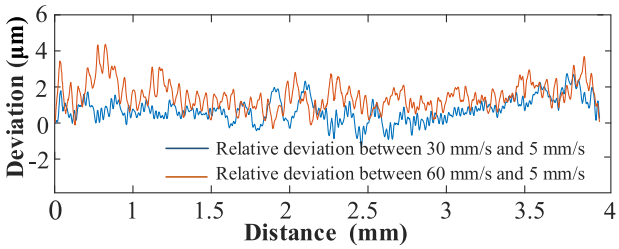

FIGURE 14. Relative deviations at different velocity.

The available second-order vibration model of the probe prototype is as Equation (10), which can better analyze the scanning parameters effectively, so as to determine the actual scanning strategy. According to the transfer function, the Bode diagram of the system is shown in Fig. 10.

$$G_s = \frac{13}{0.22s^2 + 8.9573s + 222300} \tag{10}$$

To verify the characteristics of the system response under various scanning parameters, three application experiments are designed, namely the axial runout of the linear guide (Fig. 8), the $A80l2$ sinusoidal waviness measurement (Fig. 11(a)) and the $A200l30$ curved surface measurement (Fig. 11(b)).

B. AXIAL RUNOUT OF LINEAR GUIDE

The axial runout of the linear guide is measured by the capacitive sensor (*Micro-Epsilon, CS 005*), and shown in Fig. 12, which is similar to a sine. Because there is a very tiny angle between the mirror surface and the running direction of the guide rail, the measured displacement curve appears as an inclined line. The analysis shows that the periodic amplitude of the guide rail during steady operation is about 1 μm, and the pitch of axial runout is about 170 μm.

The small pitch of the axial runout enables the allowable velocity of the guide rail to run through the **I**, **II**, and **III** stages of the velocity-amplitude curve, so the scanning velocity is set to a series of velocity from 0.2 mm/s to 16 mm/s. Fig. 13 shows the spectrum of the response signal of the probe. At 0.2 mm/s, the dominant frequency is 100.1 Hz, and the amplitude is 0.024 μm. As the scanning velocity increases, the dominant frequency and corresponding amplitude gradually increase, and achieves the maximum amplitude of 0.457 μm at 142.4 Hz, which is close to the first-order natural frequency. After that, the main frequency continues to

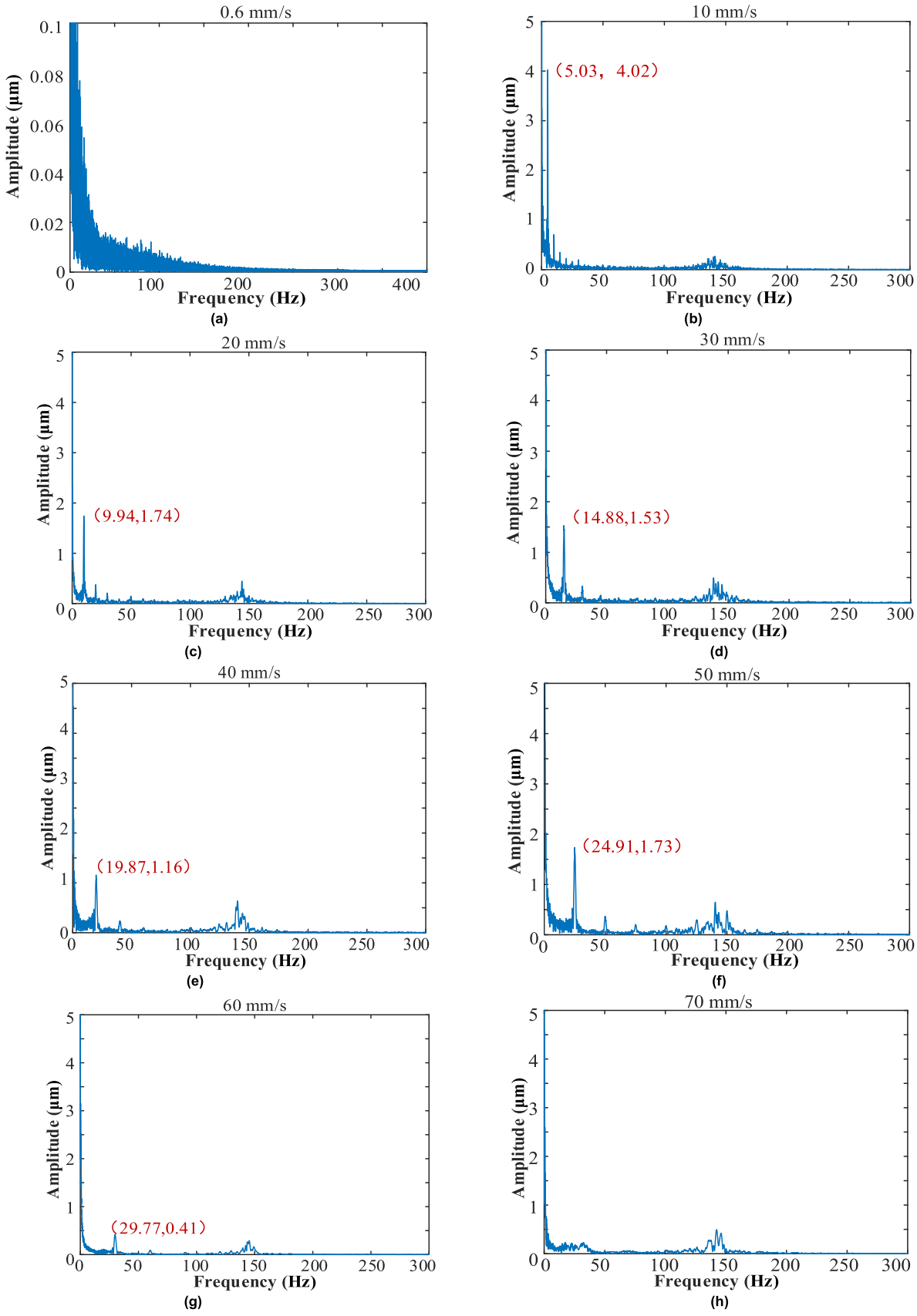

FIGURE 15. Frequency changes at different velocity.

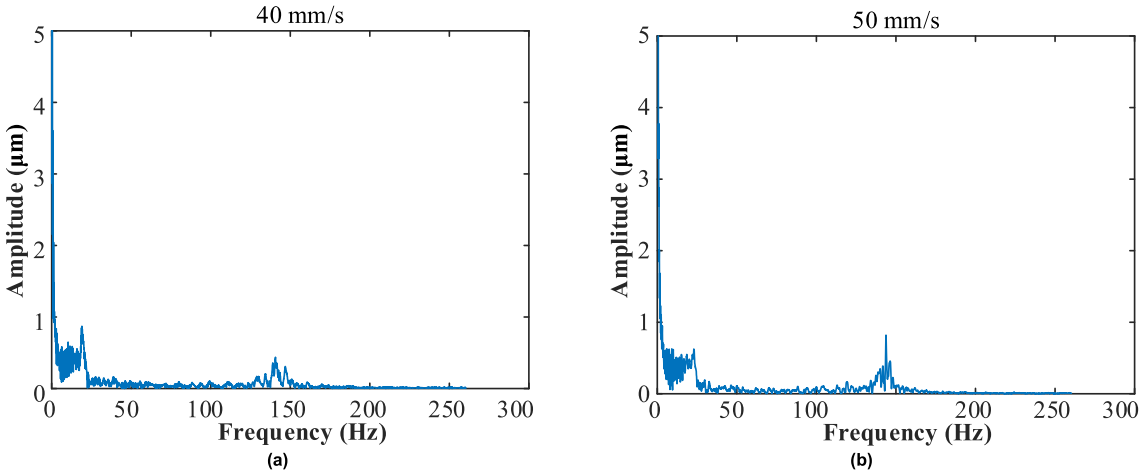

FIGURE 16. Spectrum characteristics under acceleration (a) 40 mm/s with 30 mm/s^2 (b) 50 mm/s with 30 mm/s^2.

increase slowly, but the corresponding amplitude decreases rapidly. The axial runout of the linear guide is not strictly a sine wave, although the trend of change curve of the main frequency is consistent with the theoretical analysis, it is still not significant. The second experiment will make up for this deficiency.

C. SINUSOIDAL-WAVINESS SCANNING EXPERIMENT

1) SYSTEM RESPONSE DEVIATIONS WITH VELOCITY

The design amplitude A of the sinusoidal surface is 80-100 μm, and the spacing 1 is about 2 mm. The data analysis of this experiment is carried out in the time domain and frequency domain, in which the amplitude change of the sinusoidal surface and the linear change of the dominant frequency can be observed, respectively. In the scanning velocity range of 0∼100 mm/s, the sinusoidal ripple that is not disturbed by acceleration is selected as the comparison object to study the change of amplitude. In the experiment, the relative deviations at three different velocity are compared, as shown in Fig. 14. As the velocity increases, compared to the curve at 5 mm/s, the fluctuation of the curves at the other velocity increases, meaning the deviation is bigger: the average of relative deviation under 30 mm/s is about 0.930 μm, while the deviation under 60 mm/s increases to 1.510 μm. The main reason for the increase in deviation can be seen from the Bode diagram and the velocity-amplitude curve in the theoretical analysis. The closer the velocity is to the one corresponding to the resonance frequency, the larger the amplitude in the system response will be.

According to Fig. 15, with the velocity from 0.6 mm/s to 60 mm/s, the dominant frequency of the probe response begins to change linearly from scratch to large. And the amplitude corresponding to the main frequency also shows an overall upward trend as described in theoretical analysis. Due to the influence of the axial runout of the linear guide, there is already a significant secondary frequency near 144 Hz as the velocity exceeds 2 mm/s. At low velocity, the frequency near 144 Hz is mainly caused by the axial runout of the guide rail.

In addition, the frequency spectrum corresponding to the scanning velocity at 70 mm/s has been greatly affected by the acceleration process because of the maximum acceleration limit of 200 mm/s^2. As shown in Fig. 15(h), a continuous frequency band appears between 0 and 35 Hz.

2) SYSTEM RESPONSE DEVIATIONS WITH ACCELERATION

Through theoretical analysis, the steady-state response deviation on the sine profile shows a certain increasing trend with the increase of acceleration. The amplitude and spacing parameters also affect the response deviation under acceleration. The response signal in the acceleration is a continuous frequency band in the frequency spectrum, as shown in Fig.16. The frequency band changes continuously from 0 to the corresponding frequency when the sweep is cut off. The obvious frequency appearing at about 144 Hz is caused by the axial runout of the guide rail.

The low and high acceleration experiments at two different velocity (60 mm/s, 80 mm/s) are tested. Fig. 17 shows the system response corresponding to the acceleration excitation of 20 mm/s^2, 30 mm/s^2, and 40 mm/s^2 at 60 mm/s. From the analysis of the entire scanning path, the average deviation of the whole process under the three low acceleration is very small, and there is only obvious misalignment in the corners of the peaks or valleys. The overall average deviation is less than 0.1 μm. By comparing with theory and simulation analysis, and taking into account the inherent measurement deviation of the probe, the low acceleration scanning has a small effect on the response curve.

Furthermore, the response difference between high and low accelerations of 40 mm/s^2, 80 mm/s^2 and 120 mm/s^2 matched with the velocity of 80 mm/s is studied. This experiment sets a larger acceleration interval to highlight the possible influence of acceleration on the response curve. Compared with low-velocity continuous scanning, the amplitude deviation

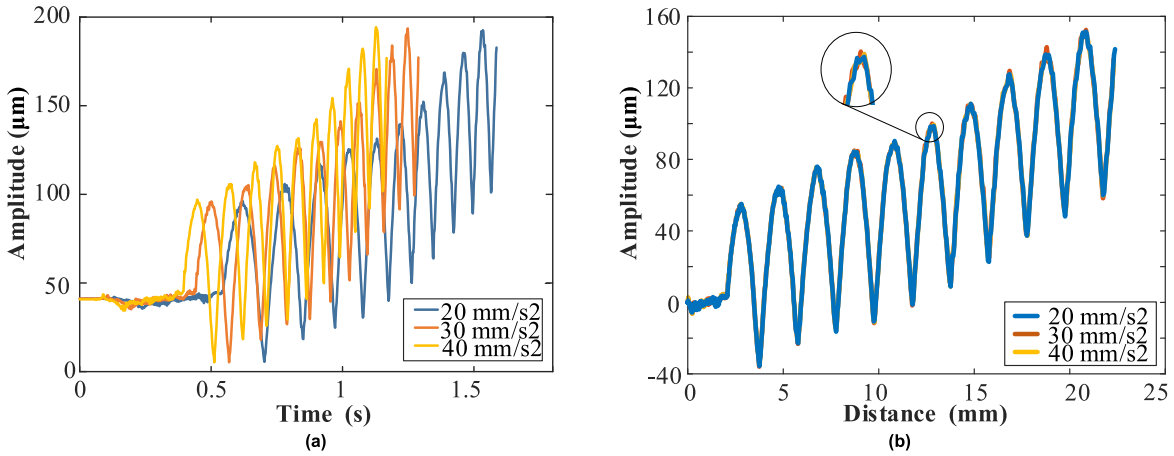

FIGURE 17. Low acceleration test at 60 mm/s (a) Time-displacement curve and (b) distance-displacement curve of the acceleration.

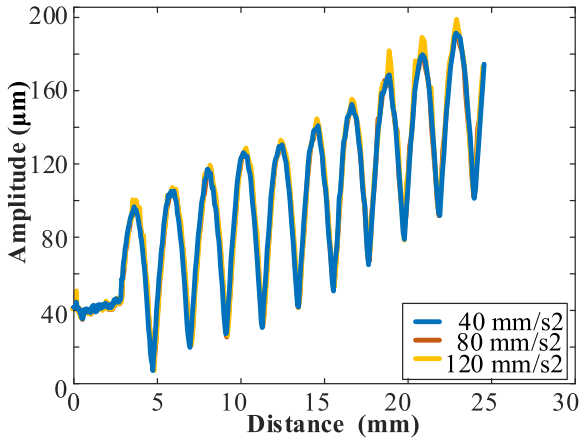

FIGURE 18. Low and high acceleration curve at 80 mm/s.

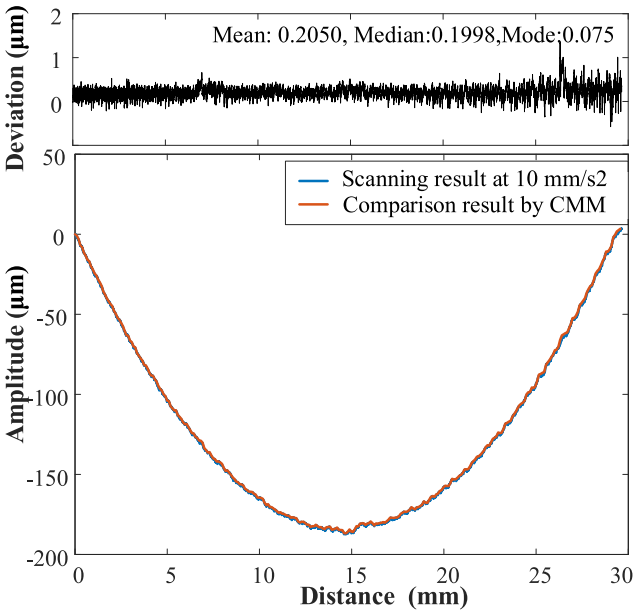

FIGURE 19. Comparative curves detected by the probe.

under high velocity scanning is significantly increased, as shown in Fig. 18. The average of relative deviations between 80 mm/s^2 and 40 mm/s^2 is about 0.620 μm, but the average between 120 mm/s^2 and 40 mm/s^2 reaches to 2.30 μm. The above is the result of removing the interference of the axial runout of the guide rail.

D. EXPERIMENTAL VERIFICATION OF LARGE CURVED SURFACE

A large arc with an amplitude A of about 200 μm and a spacing l of 30 mm is applied. According to theoretical calculations, the resonance velocity corresponding to the large curved surface is 4.784 m/s, and the amplitude deviation will reach 0.3 μm at the maximum allowable velocity of 200 mm/s of the linear guide. But in this case, the probe will sweep across the curved surface with an acceleration of no more than 200 mm/s^2 with the deviation of 0.5 μm. The considered scanning strategy is to scan across the plane on both sides of the large curved surface with an acceleration of 200 mm/s^2 and scan across the entire curved surface at a uniform velocity of 40 mm/s, of which the deviation is less than 0.08 μm. Fig. 19 represents the measurement result. Compared with the measurement curve of CMM, the average deviation of the measurement result is 0.2050 μm, the median is 0.1998 μm, and the mode is 0.075 μm. The above data is the result of compensating the systematic error including the axial runout.

V. CONCLUSION

This paper proposes a new method based on the dynamic detection of the probe system to estimate the response deviation of the probe system caused by the setting of different scanning parameters. Relying on the second-order vibration model of the real probe, the mapping relationship between the system response deviation and specific scanning variables such as velocity, acceleration and the amplitude, spacing and

curvature of the surface is quantitatively analyzed. This also makes it possible to select more appropriate scanning parameters according to the characteristics of measured objects to minimize scanning deviations.

More importantly, we realize that the dynamic characteristics of the probe, especially the natural frequency, is the key to restricting the scanning speed and acceleration. The increase of the natural frequency will make the selection range of speed and acceleration within the allowable deviation wider. But it will inevitably lead to an increase in the contact stiffness of the probe, which is not conducive to the detection of fragile surfaces. In the follow-up, we consider researching a variable stiffness probe to balance this contradiction.

REFERENCES

[1] G. Krajewski and A. Woźniak, "Simple master artefact for CMM dynamic error identification," *Precis. Eng.*, vol. 38, no. 1, pp. 64–70, Jan. 2014.

[2] A. Wozniak, G. Krajewski, and M. Byszewski, "A new method for examining the dynamic performance of coordinate measuring machines," *Measurement*, vol. 134, pp. 814–819, Feb. 2019.

[3] W. P. van Vliet and P. H. J. Schellekens, "Development of a fast mechanical probe for coordinate measuring machines," *Precis. Eng.*, vol. 22, no. 3, pp. 141–152, Jul. 1998.

[4] R.-J. Li, K.-C. Fan, Q.-X. Huang, H. Zhou, E.-M. Gong, and M. Xiang, "A long-stroke 3D contact scanning probe for micro/nano coordinate measuring machine," *Precis. Eng.*, vol. 43, pp. 220–229, Jan. 2016.

[5] T. Liebrich and W. Knapp, "New concept of a 3D-probing system for micro-component," presented at the 60th Gen. Assem. CIRP, Pisa, Italy, Aug. 2010.

[6] B. Muralikrishnan, J. A. Stone, and J. R. Stoup, "Fiber deflection probe for small hole metrology," *Precis. Eng.*, vol. 30, no. 2, pp. 154–164, Apr. 2006.

[7] M. He, R. Liu, Y. Li, H. Wang, X. Lu, G. Ding, J. Wu, T. Zhang, and X. Zhao, "Tactile probing system based on micro-fabricated capacitive sensor," *Sens. Actuators A, Phys.*, vol. 194, pp. 128–134, May 2013.

[8] K. Alblalaihid, P. Kinnell, S. Lawes, D. Desgaches, and R. Leach, "Performance assessment of a new variable stiffness probing system for micro-CMMs," *Sensors*, vol. 16, no. 4, p. 492, Apr. 2016.

[9] R.-J. Li, K.-C. Fan, J.-W. Miao, Q.-X. Huang, S. Tao, and E.-M. Gong, "An analogue contact probe using a compact 3D optical sensor for micro/nano coordinate measuring machines," *Meas. Sci. Technol.*, vol. 25, no. 9, Sep. 2014, Art. no. 094008.

[10] S. A. Farooqui and E. P. Morse, "Alternative artifacts for evaluating scanning CMM performance," presented at the ASPE Annual Meeting, Orlando, FL, USA, vol. 482, 2004.

[11] P. H. Pereira and R. J. Hocken, "Characterization and compensation of dynamic errors of a scanning coordinate measuring machine," *Precis. Eng.*, vol. 31, no. 1, pp. 22–32, Jan. 2007.

[12] A. Wozniak, "Testing the inaccuracy of CMM scanning probe," in *Proc. Int. Symp. Metrol. Qual. Control (ISMQC)*, Cariro, Egypt, 2001, pp. 57–62.

[13] A. Wozniak, "New method for testing the dynamic performance of CMM scanning probes," *IEEE Trans. Instrum. Meas.*, vol. 56, no. 6, pp. 2767–2774, Dec. 2007.

[14] F. Pollastri and A. Balsamo, "Dynamics modelling of CMM probing systems," in *Proc. Euspen's 17th Int. Conf. Exhib.*, Hannover, Germany, 2017, pp. 383–384.

[15] W. Jinwen and C. Yanling, "The geometric dynamic errors of CMMs in fast scanning-probing," *Measurement*, vol. 44, no. 3, pp. 511–517, Mar. 2011.

[16] W. Zheng, J. Guo, and Z. Liu, "A flexible-hinge touch probe using a 3D parametric model and positioning method," *Meas. Sci. Technol.*, vol. 30, no. 1, Jan. 2019, Art. no. 015001.

[17] W. Zheng and Z. Liu, "A friction-coupled measurement model of 3D scanning probe with unequal stiffness," *Meas. Sci. Technol.*, to be published, doi: 10.1088/1361-6501/abb0be.

[18] *Geometrical Product Specifications (GPS)–Surface Texture: Profile Method–Terms, Definitions and Surface Texture Parameters*, ISO Standard 12058, 1988.

[19] *Geometric Product Specifications (GPS)-Surface Texture: Profile Method: Rules and Procedures for the Assessment of Surface Texture*, ISO Standard 4287, 1997.

WEIKANG ZHENG received the B.E. degree in mechanical engineering and automation from the Ocean University of China, Qingdao, China, in 2015. He is currently pursuing the Ph.D. degree in mechanical engineering with Xi'an Jiaotong University. His research interests include the design, modeling, and control of flexible sensors, and related technology of micro/nano measurement.

ZHIGANG LIU (Member, IEEE) received the B.E. degree from the Huazhong University of Science and Technology, in 1993, the master's degree from the Xi'an University of Technology, in 1996, and the Ph.D. degree from Xi'an Jiaotong University, China, in 2000. He is currently a Professor with the School of Mechanical Engineering, Xi'an Jiaotong University. His research interests include large scale 3D measurement, frequency scanning interferometer for absolute distance measurement, external cavity diode laser, and nano-positioning.

JUNKANG GUO (Member, IEEE) received the B.S. and M.S. degrees in mechanical engineering from Central South University, and the Ph.D. degree in mechanical engineering from Xi'an Jiaotong University, Xi'an, China. He is currently an Assistant Researcher of Mechanical Engineering with Xi'an Jiaotong University. His research interests include the areas of data driven performance analysis and assembly process optimization technology for mechanical system and digital twin technology for dimensional engineering and its application.

JUN HONG (Member, IEEE) received the B.S. degree in mechanical engineering from the North University of China, Taiyuan, China, in 1989, and the M.S. and Ph.D. degrees in mechanical engineering from Xi'an Jiaotong University, Xi'an, China, in 1994 and 2001, respectively. He is currently a Professor of Mechanical Engineering with Xi'an Jiaotong University. His research interests include the area of assembly mechanism of complex precision machinery, multidisciplinary design optimization, computational mechanics, and knowledge-based engineering.